Macromolecules

ARTICLE

pubs.acs.org/Macromolecules

Unimer−Aggregate Equilibrium to Large Scale Association of Regioregular Poly(3-hexylthiophene) in THF Solution

Ye Huang, He Cheng,* and Charles C. Han*

State Key Laboratory of Polymer Physics and Chemistry, Joint Laboratory of Polymer Science and Materials, Beijing National Laboratory for Molecular Sciences, Institute of Chemistry, Chinese Academy of Sciences, Beijing 100080, P. R. China

ABSTRACT: A relatively narrow molecular weight dispersed regioregular poly(3-hexylthiophene) (*rr*-P3HT) fraction was obtained through the removal of low molecular weight fraction by Soxhlet extraction and the high molecular weight fraction by ultracentrifugation. Combined static (SLS) dynamic (DLS) light scattering and TEM measurements were conducted to study its conformation variation with temperature. An upper critical solution temperature (UCST) type of phase diagram with a loose aggregate to unimer transition process is observed in the heating process. The dynamic equilibrium between unimer, with $\langle R_h \rangle \sim 4$ nm, and loose aggregate, with $\langle R_h \rangle \sim 55$ nm, shifts to the unimer side with temperature because the loose aggregate, which consisted of bundles of unimer chains, are destroyed and dissembled by thermal energy. TEM observation was used to verify our LS results. It is found that the presence of loose aggregate in solution is crucial for the formation of interconnected and long nanofibrils in film morphology as loose aggregate embraces interchain interaction between conjugated polymer chains. Independent nanofibrils come from the crystallization of unimers during solvent evaporation process. Therefore, the percentage of interconnected nanofibrils decreases with drop-casting temperature. In the cooling process, this kinetic of self-assemble from unimers into loose aggregates in the THF solution is very slow. Taking advantage of this slow kinetic, we studied the time dependence of the structures formation at 10 °C. The unimers to loose aggregates to spherical associates to precipitates transition processes are monitored. This kinetic mapping of the unimer to loose aggregate equilibrium to nonequilibrium large scale associates is essential to optimize the nanofibrils' percentage and structure before the drop-casting process.

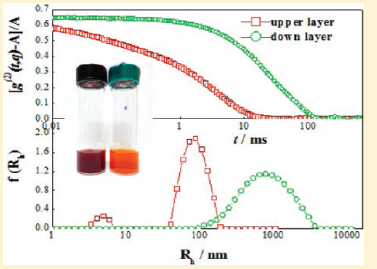

INTRODUCTION

As a potential candidate of solution-processed large-area solar cells and inkjet-printable electronic circuits, semiconductive polymers have gained more and more attention.[1−5] Poly(3-hexylthiophene) (P3HT), one of the most studied conjugated polymers, is solution-processable and exhibits excellent film-forming properties. Regioregular P3HT (*rr*-P3HT) has a relatively high charge carrier mobility (>0.1 $cm^2/(V\ s)$)[1] and is commercially available. Although we know that the molecular conformation and its self-assembly in solution could greatly influence the electro-properties of casted thin transistor film, our knowledge about the solution properties of *rr*-P3HT is still poor. Most studies indicated that conjugated polymers undergo interchain aggregation easily in the solution state, even under high dilution.[1−4] According to the report by Collison et al., poly-2-methoxy-5-(2′ethylhexoxy)phenylene-vinylene (MEH-PPV) chains are closely packed.[2] He proved the presence of "aggregate emission" in solution-casted MEH-PPV films, which competes with typical single-chromophore exciton emission and low-efficiency excimer emissions. So these "aggregates", already in existence in solutions, may survive the film-forming process and affect significantly the light emission by the generation of interchain species.[3] In this case, the interchain species looks like thermodynamically stable aggregates. While Xue et al. found that an aging process can enlarge or enrich the crystalline aggregates in *rr*-P3HT toluene solution,[5] which indicates that *rr*-P3HT toluene solution is a metastable or unstable system. Those controversial reports seem that the manufacture of a P3HT device becomes an experience governed rather than a scientifically controlled process. So it is very important to investigate its phase behavior in solution.

Original *rr*-P3HT polymerized by Grignard metathesis method cannot be narrowly distributed, the polydispersed *rr*-P3HT samples may hinder the observation of unimers to lose aggregates equilibrium because of the existence of high M_w fractions. What has induced the unknown upturn in low-*q* region reported in SANS measurements is still an open question.[11,12] Therefore, the purification of *rr*-P3HT sample is crucial before we study its solution behavior. In the last paper, we studied temperature-induced structure evolution of *rr*-P3HT in THF dilute solution and found that Soxhlet extraction process cannot give us a really narrowly dispersed, well-defined sample because it cannot remove the high molecular weight (M_w) *rr*-P3HT fraction. The high M_w fraction normally has a longer conjugated length and forms microsized precipitates when we directly dissolve it into THF.[13] So we used the ultracentrifugation to remove the closely packed microsized precipitates from the directly dissolved

Received: February 7, 2011
Revised: May 22, 2011
Published: June 02, 2011

opaque *rr*-P3HT THF solution and obtained a relatively narrowly dispersed sample.

In this article, a loose aggregates to unimers transition with temperature in *rr*-P3HT THF solution is observed by a combination of SLS, DLS, and TEM. Because SLS and DLS can give us a proper length and time scale to fully characterize the loose aggregate, while TEM can correlate the solution structure to the film morphology. Our results showed that ultracentrifugation of *rr*-P3HT THF solution after Soxhlet fraction process can really give us a relatively narrowly distributed *rr*-P3HT sample which enables us to detect its phase diagram in THF solution. According to the UCST phase diagram and Gibbs free energy landscape, the unimer and loose aggregate are in equilibrium with each other as long as the aggregate concentration has not changed through a bypass metastable process and drained into the formation of associates, so a proper control of aging time and temperature in solution can sufficiently increase the interconnected and long nanofibrils' percentage in the resultant *rr*-P3HT thin film.

EXPERIMENTAL SECTION

Materials and Methods. *rr*-P3HT was synthesized using a nickel compound as the catalyst according to the literature.[14] In order to obtain so-called narrowly dispersed, well-defined fractions, *rr*-P3HT was fractionated by Soxhlet extraction using a sequence of three solvents including methanol, *n*-hexane, and THF. All of the resultant fractions had been dried in vacuum oven for 3 days at 60 °C. After thermal treatment without ultracentrifuge, the sample with apparent $M_n = 1.6 \times 10^4$ g/mol and $M_w/M_n = 1.5$ was used in the present study. (The sample was thermal-treated to become transparent solution and then filtered before GPC measurement which was conducted at 35 °C with THF as solvent and polystyrene as standard.) The detailed GPC results will be discussed in the Results and Discussion. Tetrahydrofuran (THF) using in LS was reagent grade, bought from Sinopharm Chemical Reagent Beijing Co., Ltd., used as received. As the polymer solution which is directly prepared at room temperature looked opaque and dark purple, an enhanced method of ultracentrifugation at 10 000 rpm for 10 min was employed. All the solutions (with concentration 1 mg/mL before ultracentrifugation and filtration) were ultracentrifuged for three times using PTFE centrifugal tube. With the centrifugation being employed, the polymer solution was separated to transparent upper layer and a spot of turbid down layer. The upper layer solutions were filtered directly into the light scattering cells through 0.45 μm Millex Millipore PTFE membranes and used in the studies reported in this article. The concentration of the upper layer after filtration is 0.8 mg/mL, which is determined by UV−vis measurement according to Lambert−Beer's law.

The effect of aging on the precursor solution was also investigated by DLS and SLS. The filtered solutions using the same sample mentioned above which had been thermally treated at 55 °C to convert almost all the loose aggregate to unimers were stored in the refrigerator at 10 °C for time-resolved measurements.

Light Scattering (LS) Measurements. A commercial LS spectrometer equipped with a multi-τ digital time correlator (ALV5000) and a cylindrical 22 mW UNIPHASE He−Ne laser ($\lambda_0 = 632.8$ nm) was used. The spectrometer has a high coherence factor of $\beta \sim 0.95$ because of a novel single-mode optical fiber coupled with an efficient avalanche photodiode was used as the detector. The LS cell is held in a thermostat refractive index matching vat filled with purified and dust-free toluene, with the temperature controlled within ±0.1 °C. In static LS (SLS) the angular dependence (15°−150°) of the excess absolute time-averaged scattered intensity, i.e., the Rayleigh ratio $R_{vv}(q)$, which leads to the weight-averaged molar mass M_w and the *z*-averaged root-mean-square radius of gyration $\langle R_g^2 \rangle_z^{1/2}$ (or written as $\langle R_g \rangle$) of scattering objects,[15] where q is the scattering vector. In dynamic LS (DLS), the intensity−intensity time correlation function $g^{(2)}(t,q)$ in the self-beating mode was measured, where t is the decay time. $g^{(2)}(t,q)$ can be related to the normalized first-order electric field time correlation function $|g^{(1)}(t,q)|$ via the Siegert relation as $g^{(2)}(t,q) = A[1 + \beta|g^{(1)}(t,q)|^2]$, where A ($\equiv \langle I(0) \rangle^2$) is the measured baseline. For the broadly distributed relaxation spectrum, $|g^{(1)}(t,q)|$ is related to a characteristic relaxation time distribution $G(\tau)$, $|g^{(1)}(t,q)| \equiv \langle E(0,q)E^*(t,q) \rangle / \langle E(0,q)E^*(0,q) \rangle = \int_0^\infty G(\tau) e^{-t/\tau} d\tau$ as $G(\tau)$ can be calculated from the Laplace inversion of the measured $g^{(2)}(t,q)$.[16] When two diffusive modes were detected, they can be simply characterized by diffusion coefficients D_f, D_s, and the amplitudes A_f, A_s (subscripts f and s refer to faster and slower, respectively). A_f and A_s were evaluated through the moments of distribution functions of decay times $G(\tau)$ obtained by fitting correlation curves using CONTIN programs mentioned above. For a pure diffusive relaxation, Γ can be related to the translational diffusion coefficient D by $(\Gamma/q^2)_{C \to 0} = D$ or a hydrodynamic radius $R_h = k_B T/6\pi\eta D$ with k_B, T, and η being the Boltzmann constant, the absolute temperature, and the solvent viscosity, respectively.[16,17] The mean size of slow mode can be obtained in the Guinier regime where $I_s(q) = I_s(0) \exp(-q^2 \langle R_g \rangle_s^2/3)$, for $q\langle R_g \rangle_s < 1$. $I_s(q)$ is the scattered intensity of the slow mode at wave vector q. This equation holds regardless of refractive index or morphology and hence is very useful for determining the size of the slow mode through $\langle R_g \rangle_s$. The details of the LS instrumentation and theory can be found elsewhere.[18,19]

d*n*/d*c* Measurements. The specific refractive index increment (dn/dc) of poly(3-hexylthiophene) in THF after thermal treatment was measured by using a high-precision differential refractometer.[16] At 25 °C, the dn/dc of *rr*-P3HT in THF was 0.31 mL/g, which is close to 0.3 reported before.[20]

Transmission Electron Microscopy. Transmission electron microscopy (TEM) was performed using a JEOL 2200FS instrument at 160 kV accelerating voltage. For TEM examination, the *rr*-P3HT solution was diluted to 0.02 mg/mL and then dropped on the copper grid which is covered by carbon membrane. Subsequently, the TEM grid was placed in the vacuum oven for 12 h to remove the solvent.

RESULTS AND DISCUSSION

Effects of Ultracentrifugation. Figure 1 is the GPC results of the solution after thermal treatment and the solution after ultracentrifugation (upper layer) and thermal treatment. Note that all the samples were pretreated by Soxhlet fraction to get rid of the small molecular weight fraction. As we have mentioned in the last paper,[21] *rr*-P3HT cannot be totally dissolved in THF at room temperature; microsized precipitates can be seen by the naked eye. Most studies get rid of those precipitates by heating the opaque solution to transparent. However, thermal treatment leads the system into another metastable state. The microsized precipitates will break into spherical associates. And they are not stable at all and will precipitate again after about 9 days if they are cooled back to room temperature (RT). Because those microsized precipitates are mostly made from high M_w *rr*-P3HT fraction with longer conjugated length,[13] its general phase behavior is the same with low M_w *rr*-P3HT, but its transition point should be much higher. It was reported that the formation of P3HT precipitates with higher M_w is caused by the difunctional dimerization in the process of Grignard metathesis method catalyzed by nickel compound.[22,23] GPC measurement proved the assumption. The solid line (with $M_w = 2.4 \times 10^4$ g/mol and $M_w/M_n = 1.5$) in Figure 1 represents the molecular weight distribution of the *rr*-P3HT after thermal treatment at 55 °C without ultracentrifugation. After the ultracentrifugation

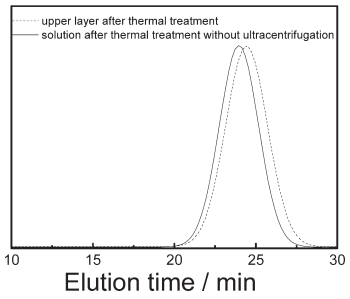

Figure 1. GPC traces of the *rr*-P3HT THF solution after thermal treatment and the solution after ultracentrifugation and thermal treatment (the upper layer solution). Solvent: THF; flow rate: 1 mL/min.

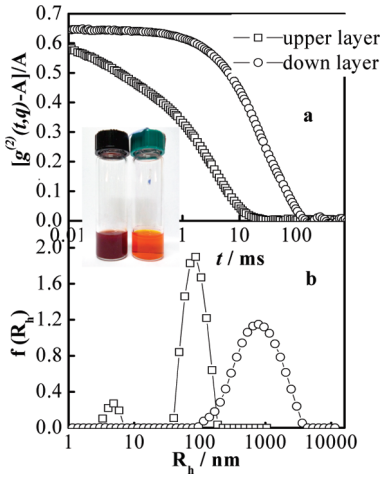

Figure 2. Intensity−intensity time correlations function $[g^{(2)}(t,q) - A]/A$ of *rr*-P3HT in THF solution (c = 0.8 mg/mL, θ = 20°, T = 20 °C): upper layer (□); down layer (○). The insert is the contrast photos of *rr*-P3HT in THF: down layer (left) and upper layer (right).

and thermal treatment, it shifted to a longer elution time which corresponds to smaller apparent M_w (dashed line with M_w = 1.9 × 10^4 g/mol and M_w/M_n = 1.4). In other words, the ultracentrifugation separated out most of the high M_w fraction which is easier to form precipitates and large associates and cannot dissolve in THF at 35 °C and be detected by GPC after thermal treatment.[21] The detailed solution structure in GPC measurement will be discussed in the Light Scattering section.

Ultracentrifugation can separate the original opaque solution into transparent upper layer and turbid dark purple down layer which were shown in the inset of Figure 2. The left cell contains the dark purple down layer which is diluted without filtration, and the right cell contains transparent upper layer after the filtration by 0.45 μm membrane. Figure 2a shows their autocorrelation functions, and Figure 2b gives correspondingly hydrodynamic radius distributions. Two modes appear in the upper layer sample. The fast mode with a dimension of ∼4 nm can be attributed to *rr*-P3HT unimers,[20] while the slow mode with a dimension of ∼55 nm coexists. However, the down layer has only one mode at low q region but two modes in high q region which means that the size of the slow mode object in down layer samples is huge, ∼1 μm (although it is not within the Rayleigh−Gans limits), and it overwhelmingly dominates the scattering profile at the low q region. So ultracentrifugation can successfully separate the precipitates which are originated from the relative

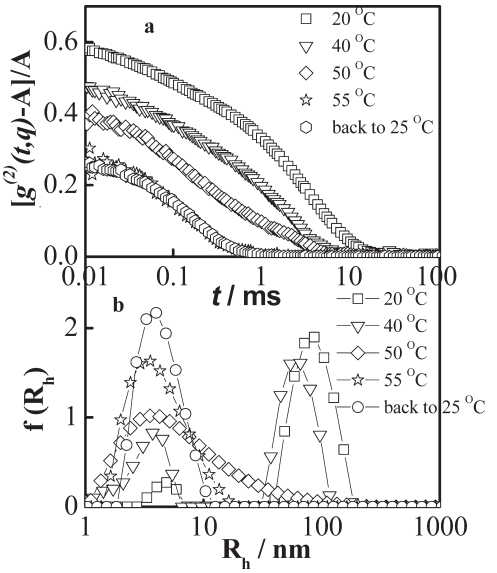

Figure 3. Temperature dependence of autocorrelation function $[g^{(2)}(t, q) - A]/A$ and the corresponding hydrodynamic radius distributions of the upper layer in the first heating process (θ = 20°).

high M_w fractions. After extracting the very low M_w fractions by Soxhlet fraction process and removing the higher M_w fractions by ultracentrifugation, we obtained a relatively narrowly distributed *rr*-P3HT sample, which is in principle thermodynamically stable at room temperature and exhibits clear phase transition process with temperature between unimers and assembled structure. However, we will show in following sections that the assembled structure is still in a metastable state, which can be converted to associates in a slow transformation and then to an even larger aggregate state eventually at lower temperature.

DLS Measurement of *rr*-P3HT Conformation in the Upper Layer during First Heating Process. The temperature-dependent conformation variation of *rr*-P3HT in the upper layer can be measured by DLS. Figure 3a shows the temperature dependence of autocorrelation functions, and Figure 3b gives their corresponding hydrodynamic radius distribution in the first heating process. At room temperature, two modes appear. The fast mode, with a dimension of ∼4 nm, is a measure of *rr*-P3HT unimer while the slow mode with a dimension of $\langle R_h \rangle_s$∼ 55 nm is a measure of interchain assembled structure due to strong $\pi-\pi$ interaction between *rr*-P3HT segments. The percentage of the slow mode decreases with temperature. This slow mode almost disappears and leaves with a broad distributed fast mode at 50 °C and above, which means that it is a UCST process. The increase of temperature favors *rr*-P3HT−solvent interaction and breaks $\pi-\pi$ interaction between *rr*-P3HT segments. It also proves that ultracentrifugation, instead of thermal treatment at high temperature, purifies *rr*-P3HT much better. The relatively narrowly distributed *rr*-P3HT makes the observation of its real phase behavior possible. Although it is a UCST phase diagram, i.e., assembled structure breaks into unimer with temperature, the re-equillibrium with unimer and assembled structure is extremely slow in the cooling process. It takes more than 4 h for us to detect the reappearance of the assembled structure at RT in DLS measurement. Therefore, the dashed line in Figure 1 can really reflect the *rr*-P3HT molecular weight distribution in solution.

dx.doi.org/10.1021/ma200273u |*Macromolecules* 2011, 44, 5020–5026

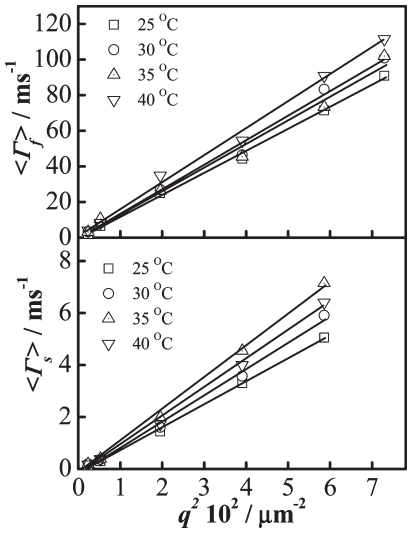

Figure 4. Temperature dependence of average characteristic line width $\langle\Gamma\rangle$ vs q^2 in the upper layer of the dilute *rr*-P3HT solution: (a) the fast diffusive relaxation mode; (b) the slow diffusive relaxation mode.

A temperature dependence of decay time $\langle\Gamma\rangle$ vs q^2 is presented in Figure 4. For purely diffusive relaxation in dilute solution, $\langle\Gamma\rangle$ is linearly dependent on the square of the scattering vector q, passing through the origin. A straight line passing through the origin reveals that both relaxation modes are purely diffusive in the temperature range from 20 to 45 °C. In the observable temperature range, the fast mode is the diffusive motion of *rr*-P3HT unimer, while the slow mode may be attributed to the diffusive motion of certain structure, and it will be discussed in the next section.

SLS Determination of the Basic Shape and Temperature Evolution of Slow Mode Object in the Upper Layer. Figure 5a, b shows the temperature dependence of $\langle R_g\rangle_s$, $\langle R_h\rangle_s$, and $\langle R_g\rangle_s/\langle R_h\rangle_s$ in a heating process. Theoretically, there are two ways to define the shape of the assembled structure in solution, namely, combined static and dynamic light scattering (SLS and DLS) and small-angle neutron scattering (SANS), respectively. Both of them are strongly model-dependent, and the former is much easier if the dimension of the subject being studied is within the q range of light scattering. Because it is a polydisperse multicomponent system and the poor q resolution, we did not use SANS to determine its basic shape. In fact, the structure of the slow mode object can be simply viewed from the ratio between $\langle R_g\rangle_s$ and $\langle R_h\rangle_s$. This is because they are related to the segmental distribution in different ways: $\langle R_g\rangle$ is related to the square average of the segmental distribution $\langle r_{ij}^2\rangle$ and reflects the density distribution in real space, while $\langle R_h\rangle$ is related to the inverse segmental distribution $\langle r_{ij}^{-1}\rangle$ and is the radius of an equivalent nondraining sphere with the same translational diffusion coefficient (demonstrated as $\rho = \langle R_g\rangle/\langle R_h\rangle = [1/(2N^2)\sum_{n=1}^{N}\sum_{m=1}^{N}\langle(r_n - r_m)^2\rangle]^{1/2}\langle 1/(|r_n - r_m|)\rangle$). For random coil, hyperbranched cluster, and uniform sphere, $\langle R_g\rangle/\langle R_h\rangle$ is 1.5−1.8, 1.0−1.2, and ∼0.8, respectively.[24] The values 1.5 and 1.73 correspond to a narrowly dispersed and polydispersed Gaussian coil in theta solvent, respectively. We can find that during the whole heating process as the slow mode exists $\langle R_g\rangle_s/\langle R_h\rangle_s$ of the slow mode decreases from ∼1.8 to ∼1.5. The backbone of polythiophene is not soluble in any solvent, and then the solubility of poly(3-hexylthiophene) (P3HT) is enhanced by the hexyl side group.

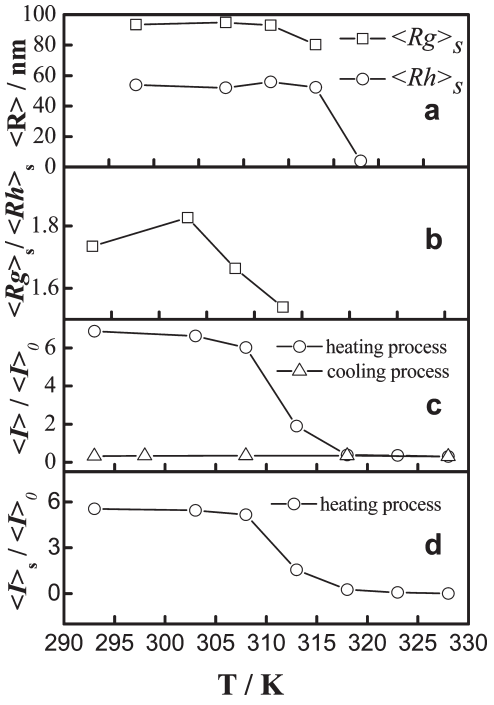

Figure 5. Temperature dependence of (a) the average radius of gyration and hydrodynamic radius, (b) their ratio of the slow mode in the upper layer, (c) total normalized total scattered light intensity, and (d) normalized scattered light intensity of the slow mode contribution ($\theta = 20°$).

Therefore, P3HT contains both solvophilic side groups and solvophobic backbone, and several assembled structures in different length scales can be formed. Combined with the result in Figure 4, the motion of the assembled structure is purely diffusive; we may conclude that the slow mode object is a loose aggregate in which the strong $\pi-\pi$ interaction between thiophene segments makes P3HT chains loosely bundle together. The high regioregular configuration induces strong $\pi-\pi$ stacking between *rr*-P3HT segments and makes *rr*-P3HT chains bundle together to form this loose aggregate. The decrease of $\langle R_g\rangle_s/\langle R_h\rangle_s$ ratio from ∼1.8 to ∼1.5 reveals that its aggregated backbone gets more and more flexible with temperature. The further increase of temperature dissolves loose aggregate, and the $\langle R_g\rangle$ of the unimer is too small to show any angular dependent scattered light intensity.

Figure 5c,d shows the temperature evolution of the normalized total scattered light intensity $\langle I\rangle/\langle I\rangle_0$ and the scattered light contribution of the slow mode $\langle I\rangle_s/\langle I\rangle_0$, where $\langle I\rangle$ is the scattered light intensity at $\theta = 20°$ and $\langle I\rangle_0$ is the incident light intensity. The total average scattered light intensity ($\langle I\rangle$) comes from the summation contributions from unimers $\langle I\rangle_f$ and loose aggregate $\langle I\rangle_s$, where the solvent contribution has been omitted, namely, with $\langle I\rangle = \langle I\rangle_f + \langle I\rangle_s$ and $\langle I\rangle_f = \langle I\rangle A_f$, $\langle I\rangle_s = \langle I\rangle A_s$, and $A_f + A_s = 1$, with A_f and A_s are the intensity weight fractions of the fast and slow modes, respectively. Note that the $\langle I\rangle/\langle I\rangle_0$ at $\theta = 20°$ is contributed by both unimer and loose aggregate scattering, but the scattering at $\theta = 20°$ is dominated by the scattering from the large loose aggregate; therefore, we used the notation $\langle I\rangle_s/\langle I\rangle_0$ in Figure 5d. At room temperature, the dynamic coexistence of unimer and loose aggregate makes both $\langle I\rangle/\langle I\rangle_0$ and $\langle I\rangle_s/\langle I\rangle_0$ relatively high. Their ratios are decreasing with temperature

dx.doi.org/10.1021/ma200273u |*Macromolecules* 2011, 44, 5020–5026

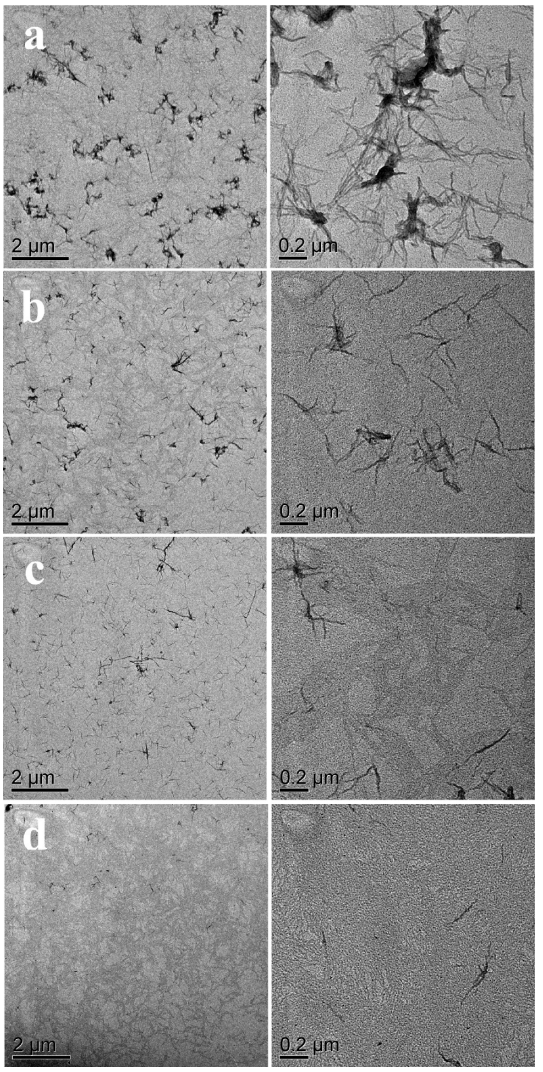

Figure 6. TEM micrographs depicting morphology evolutions of drop-casted *rr*-P3HT films of the upper layer at different solution temperatures: (a) 20, (b) 40, (c) 50, and (d) 55 °C at two different levels of magnification.

because the dynamic equilibrium shifts severely to the unimer side; i.e., it is a UCST process in nature. The solubility of loose aggregate gets better; it releases more and more unimers with temperature. At 55 °C, it is uniformly one phase, and only unimers exist. Note that $\langle I\rangle/\langle I\rangle_0$ almost keeps a constant for more than 1 h in the cooling process, which indicates that it is a slow kinetic process for unimers to reassemble into the loose aggregate.

TEM Evaluation of *rr*-P3HT Upper Layer Structure Influence on the Morphology of Casted Films. The memory of chain conformation in solution can be carried into its casted film. Figure 6 shows the TEM micrographs of nanocrystalline morphologies of *rr*-P3HT thin film after drop-casting from the upper layer solution at different temperatures. The average width of the nanofibril crystal domains maintains about 18 ± 4 nm,[25,26] while its length strongly depends on the drop-casting temperature. At lower temperature, interconnected and long nanofibrils are observed. At high temperature especially at 55 °C, only independent short nanofibrils exist in the thin film.

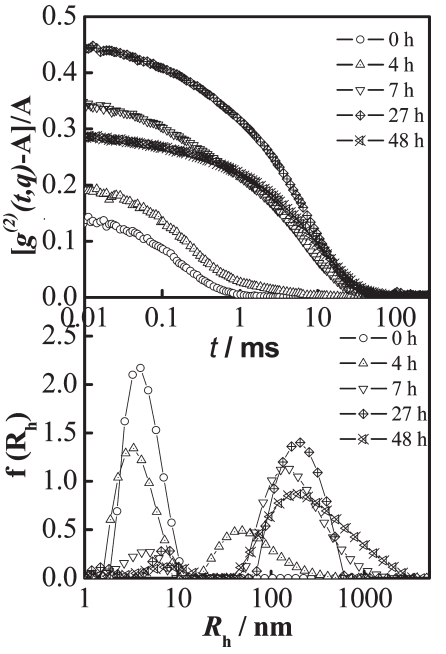

Figure 7. Time-resolved autocorrelation function $[g^{(2)}(t,q) - A]/A$ (a) and the corresponding hydrodynamic radius distributions of the upper layer (b) at 10 °C just after thermal treatment at 55 °C for 30 min (θ = 20°).

The presence of loose aggregate is crucial for the formation of interconnected nanofibrils. The *rr*-P3HT fractions with a relatively narrowly distributed M_w have a UCST type of phase diagram. On one hand, the phase boundary between each metastable state is not very clear, i.e., loose aggregates and unimers coexist in a large temperature range; on the other hand, an increase of *rr*-P3HT concentration via solvent evaporation also increases the loose aggregate population according to the UCST phase diagram. At lower temperature, the solvent evaporation rate is very low, and the loose aggregate population in THF solution is relatively high. It can serve as the nucleation sites for unimers, and its intermolecular $\pi-\pi$ stacking possibly enhances the formation of elongated and interconnected nanofibrils. On the contrary, only *rr*-P3HT unimers exist at higher temperature; the faster solvent evaporation rate gives the polymer chain little time to adjust their conformation to form loose aggregate. Only very short and independent nanofibrils can be observed on the drop-casted *rr*-P3HT films at 55 °C.

Aging Effects. As we have mentioned above, there is an obvious slow kinetic process during the first cooling cycle; i.e., the *rr*-P3HT conformation in THF solution just after temperature drop did almost not change in 1 h compared with that at 55 °C. In order to speed up the phase separation process, we further cooled the sample to 10 °C and studied the aging effect on *rr*-P3HT conformational transformation in THF.

Figure 7 shows the autocorrelation function $[g^{(2)}(t,q) - A]/A$ and the corresponding hydrodynamic radius distribution of the unimer and assembled structure in the solution after cooled down to 10 °C as a function of aging time. At the very beginning, the correlation function has only one fast mode which can be attributed to the diffusion of unimer. After 4 h, an obvious slow mode tail appears in the autocorrelation function, and its hydrodynamic radius $\langle R_h\rangle$ is ~65 nm. Both the percentage and the size of the slow mode increase with time. The relative width

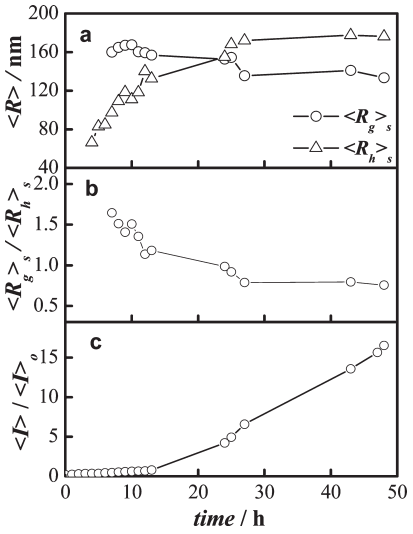

Figure 8. Time-resolved (a) the average radius of gyration and hydrodynamic radius, (b) their ratio of the slow mode, and (c) the normalized total scattered light intensity in the upper layer at 10 °C (θ = 20°).

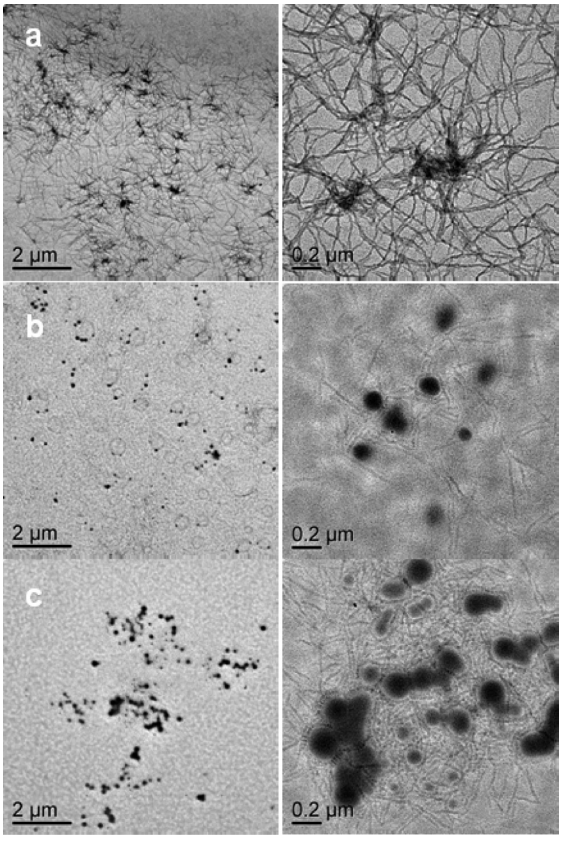

Figure 9. TEM micrographs depicting morphology evolutions of drop-casted *rr*-P3HT films of the upper layer at different aging time at 10 °C: (a) 10, (b) 46, and (c) 109 h at two different levels of magnification.

of the slow mode distribution is broadening, too. Precipitates that can be seen by the naked eye will appear after 4 days.

Figure 8 records the time dependence of (a) the average radius of gyration $\langle R_g \rangle_s$, the average hydrodynamic radius $\langle R_h \rangle_s$, (b) their ratio $\langle R_g \rangle_s / \langle R_h \rangle_s$, and (c) the normalized total scattered

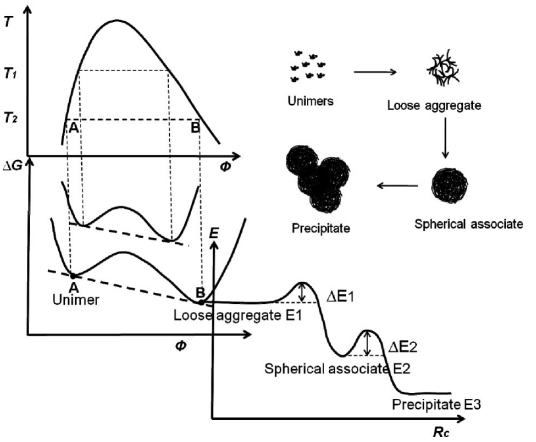

Figure 10. Schematic representation of UCST type phase diagram and Gibbs free energy landscape in illustrating the phase pathways and energy levels of each metastable states with critical nuclei size (left) of the upper layer of *rr*-P3HT solution. The illustration of the assembled structures in the corresponding states (right).

light intensity at θ = 20° in the upper layer at 10 °C after different aging times. At first, angular independent scattered light intensity shows no $\langle R_g \rangle_s$. As time goes by, the scattered light intensity is increasing, which indicated self-assemble process begins. $\langle R_h \rangle_s$ becomes ~65 nm and increases with time, while the ratio $\langle R_g \rangle_s / \langle R_h \rangle_s$ decreases from ~1.6 to ~0.8. At 7 h, loose aggregates form first ($\langle R_g \rangle_s / \langle R_h \rangle_s \sim 1.6$). After that, at 27 h, the further collapse of the loose aggregate induces the formation of spherical associates which are densely packed ($\langle R_g \rangle_s / \langle Rh \rangle_s \sim 0.8$). Finally, micro-sized precipitates can be seen by the naked eye, and the total scattering intensity starts to decrease probably due to the precipitation of microsized particles falling off the solution.

Figure 9 shows the TEM micrographs of the drop-casting films at different aging time at 10 °C. At 10 h, loose aggregates and unimers coexist in solution; the percentage of loose aggregates can further increase easily during slow evaporation process. So the population of interconnected and long nanofibirils is quite high. While at 46 h, the unimer percentage is lower, and the loose aggregates are collapsing and associating to form spherical associates (as seen in Figures 7 and 8), so a small number of spherical associates appear. Finally, at 109 h, most unimers have already converted into spherical associates; they collide to form some fractal precipitates while keeping their basic spherical shape. Obviously, to enhance the population of interconnected and long nanofibrils in the drop casted *rr*-P3HT films, a proper thermal treatment and aging process are crucial. The casting has to be done before the loose aggregate begins to collapse and precipitate.

The whole process can be schematically illustrated in Figure 10. In this study, relatively narrowly distributed *rr*-P3HT was obtained after Soxhlet extraction and ultracentrifugation of directly dissolved *rr*-P3HT opaque THF solution. Figure 10 (left) represents Gibbs free energy vs volume fraction at a given temperature, and the coexistence points on the binodal line can be obtained from the common tangent. We should stress that this is just a pseudo-two-phase system (actually the two coexistence phases should be unimer solution and loosely aggregate structure with solvent inside)[27,28] because the aggregate part will never fully phase separate into macroscopic single domain. Benedek proposed a thermodynamic theory of phase separation in

self-associating micellar solution,[27] and Einaga proved the micellar solution can be substantially treated as binary systems although the micelles in solution may have distribution in size and multiple equilibriums are established among them.[29] In this study, stable unimer and metastable loose aggregate with the same chemical potential coexist at room temperature, as points A and B shown in Figure 10 (left). Temperature elevation can shift the balance severely to the unimer side because it is a UCST type phase diagram as indicated by the T_1 case in Figure 10, which is the origin of loose aggregate to the unimer transition. However, in the cooling process, the energy barrier between stable unimer state and metastable loose aggregate state may be somewhat higher than kT, which makes it a slower kinetic process for the equilibrium transition. Meanwhile, the lower temperature such as T_2 can make it easier for the loose aggregate to transform to metastable states at even lower energy states, e.g., first to the spherical associates and then to the aggregated precipitates which are demonstrated in Figure 10 (right). Although the loose aggregate is in an equilibrium state with the unimer state, it is also metastable and possible to transfer to a lower energy spherical associate which in turn can transform to aggregated precipitates with even lower energy, and this forms the physical pathway of the aging process.

CONCLUSION

The THF dilute solution of regioregular poly(3-hexylthiophene) (*rr*-P3HT) was separated into transparent upper layer and turbid dark purple down layer by ultracentrifugation. The light scattering characterization of the upper layer has shown that unimers and loose aggregates coexist in the upper layer solution at room temperature. The loose aggregate can dissolve and transform into unimers during the heating process so it is a UCST phase diagram. The reversible kinetic process, although it is slow, was obtained as the unimers return to the loose aggregates, then to spherical associates, and finally the microsized precipitates during the aging process at 10 °C. TEM characterization of the drop-casted film morphology has confirmed these transitions because the corresponding chain conformation is carried into film morphology. We believe a proper control of solution temperature, concentration, and aging time is crucial to enhance electro-optical properties of the final devices.

AUTHOR INFORMATION

Corresponding Author

*E-mail: c.c.han@iccas.ac.cn (C.C.H.), chenghe@iccas.ac.cn (H.C.); Tel: +86-10-8261-8089; Fax: +86-10-6252-1519.

ACKNOWLEDGMENT

The financial support from the National Natural Science Foundation of China (Young Scientists Fund) (20804052) and the Institute of Chemistry Chinese Academy of Sciences (CMS-LX200921) is gratefully acknowledged.

REFERENCES

(1) Grell, M.; Bradley, D. D. C.; Long, X.; Chamberlain, T.; Inbasekaran, M.; Woo, E. P.; Soliman, M. *Acta Polym.* **1998**, *49* (8), 439–444.

(2) Collison, C. J.; Rothberg, L. J.; Treemaneekarn, V.; Li, Y. *Macromolecules* **2001**, *34* (7), 2346–2352.

(3) Chen, S. H.; Su, A. C.; Huang, Y. F.; Su, C. H.; Peng, G. Y.; Chen, S. A. *Macromolecules* **2002**, *35* (11), 4229–4232.

(4) Nguyen, T. Q.; Doan, V.; Schwartz, B. J. *J. Chem. Phys.* **1999**, *110* (8), 4068–4078.

(5) Xue, L.; Gao, X.; Zhao, K.; Liu, J.; Yu, X.; Han, Y. *Nanotechnology* **2010**, *21* (14), 145303.

(6) Dreiss, C. A. *Soft Matter* **2007**, *3* (8), 956–970.

(7) Hashizaki, K.; Taguchi, H.; Saito, Y. *Colloid Polym. Sci.* **2009**, *287* (9), 1099–1105.

(8) Jeong, J. H.; Kang, H. S.; Yang, S. R.; Kim, J. D. *Polymer* **2003**, *44* (3), 583–591.

(9) Nam, Y. S.; Kang, H. S.; Park, J. Y.; Park, T. G.; Han, S. H.; Chang, I. S. *Biomaterials* **2003**, *24* (12), 2053–2059.

(10) Sommer, C.; Pedersen, J. S.; Egelhaaf, S. U.; Cannavacciuolo, L.; Kohlbrecher, J.; Schurtenberger, P. *Langmuir* **2002**, *18* (7), 2495–2505.

(11) Aime, J. P.; Bargain, F.; Schott, M.; Eckhardt, H.; Miller, G. G.; Elsenbaumer, R. L. *Phys. Rev. Lett.* **1989**, *62* (1), 55–58.

(12) Li, Y. C.; Chen, C. Y.; Chang, Y. X.; Chuang, P. Y.; Chen, J. H.; Chen, H. L.; Hsu, C. S.; Ivanov, V. A.; Khalatur, P. G.; Chen, S. A. *Langmuir* **2009**, *25* (8), 4668–4677.

(13) Rughooputh, S. D. D. V.; Hotta, S.; Heeger, A. J.; Wudl, F. *J. Polym. Sci., Part B: Polym. Phys.* **1987**, *25* (5), 1071–1078.

(14) Loewe, R. S.; Khersonsky, S. M.; McCullough, R. D. *Adv. Mater.* **1999**, *11* (3), 250–253.

(15) Wang, J.; Wang, Z. L.; Peiffer, D. G.; Shuely, W. J.; Chu, B. *Macromolecules* **1991**, *24* (3), 790–798.

(16) Wu, C.; Xia, K. Q. *Rev. Sci. Instrum.* **1994**, *65* (3), 587–590.

(17) Wu, C.; Zhou, S. Q. *J. Polym. Sci., Part B: Polym. Phys.* **1996**, *34* (9), 1597–1604.

(18) Chu, B. *Laser Light Scattering*; Academic Press: New York, 1974.

(19) Berne, B. J.; Pecora, R. *Dynamic Light Scattering*; Plenum Press: New York, 1976.

(20) Heffner, G. W.; Pearson, D. S. *Macromolecules* **1991**, *24* (23), 6295–6299.

(21) Huang, Y.; Cheng, H.; Han, C. C. *Macromolecules* **2010**, *43* (23), 10031–10037.

(22) Iovu, M. C.; Sheina, E. E.; Gil, R. R.; McCullough, R. D. *Macromolecules* **2005**, *38* (21), 8649–8656.

(23) Miyakoshi, R.; Yokoyama, A.; Yokozawa, T. *J. Am. Chem. Soc.* **2005**, *127* (49), 17542–17547.

(24) Burchard, W., Brown, W., Eds.; Clarendon Press: Oxford, 1996; p 439.

(25) Kline, R. J.; McGehee, M. D.; Kadnikova, E. N.; Liu, J. S.; Frechet, J. M. J.; Toney, M. F. *Macromolecules* **2005**, *38* (8), 3312–3319.

(26) Wang, W.; Lieser, G.; Wegner, G. *Makromol. Chem., Macromol. Chem. Phys.* **1993**, *194* (5), 1289–1297.

(27) Blankschtein, D.; Thurston, G. M.; Benedek, G. B. *Phys. Rev. Lett.* **1985**, *54* (9), 955–958.

(28) Pacheco-Sanchez, J. H. *Rev. Mex. Fis.* **2001**, *47* (4), 324–338.

(29) Yoshimura, S.; Shirai, S.; Einaga, Y. *J. Phys. Chem. B* **2004**, *108* (40), 15477–15487.